

Resonance Patterns in a Stadium-shaped Microcavity

Soo-Young Lee,* M. S. Kurdoglyan, Sunghwan Rim, and Chil-Min Kim†
*National Creative Research Initiative Center for Controlling Optical Chaos,
Pai-Chai University, Daejeon 302-735, Korea*

We investigate resonance patterns in a stadium-shaped microcavity around $n_c k R \simeq 10$, where n_c is the refractive index, k the vacuum wavenumber, and R the radius of the circular part of the cavity. We find that the patterns of high Q resonances can be classified, even though the classical dynamics of the stadium system is chaotic. The patterns of the high Q resonances are consistent with the ray dynamical consideration, and appears as the stationary lasing modes with low pumping rate in the nonlinear dynamical model. All resonance patterns are presented in a finite range of kR .

PACS numbers: 42.55.Sa, 42.65.Sf, 05.45.Mt

I. INTRODUCTION

As a central concept of the promising photonics technology, recently microcavity has attracted much attention due to its necessity for the generation and switching of coherent light[1]. In a cylindrical and spherical dielectric cavities, light trapped by total internal reflection can make very high Q modes, so-called whispering gallery modes (WGM). Lasing of WGM has been studied extensively[2, 3, 4, 5]. Imposing small deformation on circular and spherical symmetric cavities, one can obtain lasing modes with directional emission which is more useful for the potential application to photonics[6, 7].

It is known that even in chaotic microcavities the lasing modes with high Q and very good directionality can be excited[8]. There are several reports for observation of scarred lasing modes in various microcavities whose patterns show enhanced field intensity along an unstable periodic orbit of the cavity[9, 10, 11, 12]. Moreover, due to the inherent properties of the dielectric cavities, the existence of quasi-scarred resonance modes[13], which are not supported by any unstable periodic orbit, are suggested and numerically confirmed in a spiral-shaped dielectric microdisk. In a nonlinear dynamical model of a stadium-shaped cavity with an active medium, Harayama et al. examined laser action on a single spatially chaotic wave function[14] and locking of two resonance modes of different symmetry classes and slightly different frequencies[15].

In this paper we study resonances of the stadium-shaped microcavity by using the boundary element method (BEM)[16]. We present the whole resonances in the range of $8 < \text{Re}(n_c k R) < 11$ with the refractive index $n_c = 2$ to show what resonance patterns are possible to appear as lasing modes and to find the relationships between Q factor and resonance pattern. We note that the classical dynamics of the stadium-shaped billiard is chaotic. This means that the resonances cannot

be classified by mode indices, similar to the absence of good quantum number in quantum mechanical problem. In spite of its chaotic ray dynamical properties, we find that the high Q modes in this $\text{Re}(n_c k R)$ range have special patterns which can be classified from other modes, and these modes are really excited with low pumping rate in the nonlinear dynamical model developed in [14].

This paper is organized as follows. In Sec.II we summarize the BEM used to obtain resonances numerically, and the resulting resonances are presented and discussed in Sec.III. In Sec.IV the variations of the resonance position and pattern with the refractive index n_c are discussed. We confirm, in Sec.V, the fact that the high Q resonances are the stationary modes with low pumping rate in the nonlinear dynamical model, and a ray dynamical consideration for the high Q resonance patterns is given in Sec.VI. Finally we summarize results in Sec.VII.

II. BOUNDARY ELEMENT METHOD

In this section we briefly describe the boundary element method (BEM)[16] which is effective when the boundary is strongly deformed from a circular shape. In the microdisk case, Maxwell's equations can be reduced to a two-dimensional Helmholtz equation

$$(\nabla^2 + n(\mathbf{r})^2 k^2) \psi = 0. \quad (1)$$

The main idea of BEM is to replace the Helmholtz equation by one-dimensional boundary equations and then to discretize the boundaries. To obtain the one-dimensional boundary equation, the Green function, the solution of the Helmholtz equation with a delta function source, and Green's identity are used. The Green function for the Helmholtz equation is given by the zeroth-order Hankel function of the first kind,

$$G(\mathbf{r}, \mathbf{r}'; nk) = -\frac{i}{4} H_0^{(1)}(nk|\mathbf{r} - \mathbf{r}'|). \quad (2)$$

Then the resulting boundary integral representation is

$$c\psi(\mathbf{r}) = \oint_{\Gamma} ds' [\partial_{\nu} G(\mathbf{r}, s'; nk) \psi(s') - G(\mathbf{r}, s'; nk) \partial_{\nu} \psi(s')], \quad (3)$$

*Electronic address: sooyoung@phys.paichai.ac.kr

†Electronic address: chmkim@mail.paichai.ac.kr

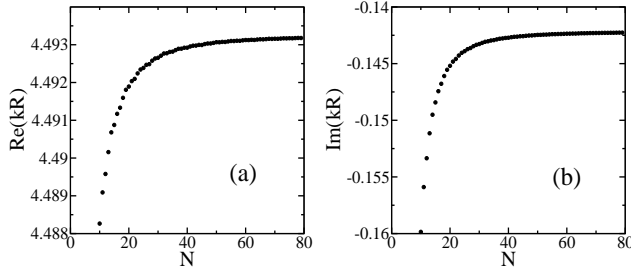


FIG. 1: Convergence of the solution kR for the resonance OO_3 with the number of elements on the boundary. (a) Real part (b) Imaginary part

where c is 1 for \mathbf{r} inside the boundary Γ , $1/2$ for \mathbf{r} on the boundary, 0 otherwise, and ∂_ν means the outward normal derivative at the boundary. In our case the boundary is a simple stadium shape, we can therefore make, by locating \mathbf{r} on the boundary, two boundary equations corresponding to the inside and outside of the microdisk, respectively. Discretization of the two boundary equations leads to a matrix equation,

$$\mathbf{M} \begin{pmatrix} \psi \\ \partial_\nu \psi \end{pmatrix} = 0, \quad (4)$$

where (ψ) and $(\partial_\nu \psi)$ are column vectors composed by the values of ψ and $\partial_\nu \psi$ at the element points on the boundary. The non-trivial solution of this matrix equation exists only when the determinant of \mathbf{M} is zero, which is the condition used in determining the complex wavenumber k of resonances.

Note that Hankel functions in the Green function and its normal derivative are singular at the origin, so a careful treatment is needed to overcome this singularities. The singularity of $H_1^{(1)}(z)$ in $\partial_\nu G$ can be compensated by a geometrical factor, and the corresponding diagonal terms can be expressed in terms of the curvature κ of the boundary. In order to treat the singularity of $H_0^{(1)}(z)$ in G , we use the asymptotic expression of $H_0^{(1)}(z)$ and integrate it in the related elements[16].

In this paper, we focus on TM polarization where both the wavefunction ψ and its normal derivative $\partial_\nu \psi$ are continuous across the boundary, and the ψ corresponds to z -component of electric field E_z when the disk lies on x - y plane. In the case of TE polarization, the ψ represents the magnetic field H_z and the wavefunction ψ is continuous across the boundary, but its normal derivative is not, instead, $n(\mathbf{r})^{-2} \partial_\nu \psi$ is continuous. This boundary condition can be incorporated into the above formalism by a slight correction. In practical calculations we take into consideration of the symmetry of the stadium-shaped microcavity, i.e., stadium has symmetries about the x - and y -axes. The symmetry consideration leads to the reduction of computing time by allowing to treat only quarter part of the stadium boundary. Instead we have to use the desymmetrized Green function when constructing the matrix equation Eq.(4).

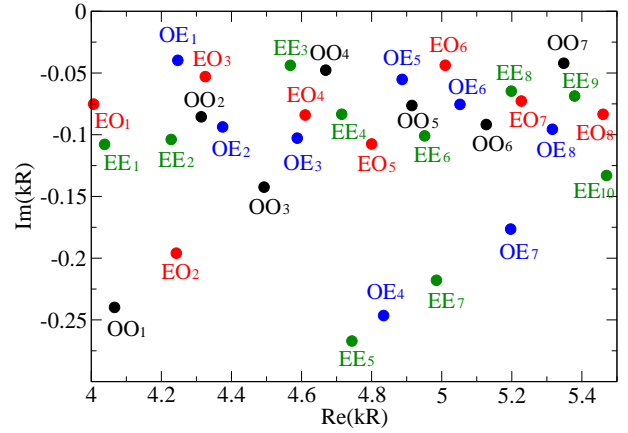


FIG. 2: (Color online) Resonance points in the complex kR space. Black, red, blue, and green points represent resonances of odd-odd, even-odd, odd-even, and even-even symmetric class, respectively. The numbering starts from the smallest $\text{Re}(kR)$ value.

Generally the space between element points can be taken as a variable of the curvature, i.e., if the curvature is large, then take a large number of points. The stadium-shaped boundary is, however, simple enough to take equal spacing points. In the practical calculation we take 50 elements on the quarter part of the boundary, which corresponds to about 12 element per a wavelength ($\lambda_c = 2\pi/n_c k$). Fig.1 shows the convergence of the complex k value of the resonance OO_3 (see Fig.2) with the number of elements N in the quarter part of the boundary. The values at $N = 50$ gives an error less than 0.2 % from the limit values.

III. RESONANCES IN STADIUM-SHAPED MICROCAVITY

We find 33 resonances in the range $8 < n_c kR < 11$ with $n_c = 2$. The number of resonances in this range can be inferred from the modified Weyl's theorem[17],

$$N_0(k) \simeq \frac{Ak^2}{4\pi} \mp \frac{Lk}{4\pi} + \frac{1}{2\pi} \int_\Gamma ds \kappa(s) + \dots, \quad (5)$$

where A is the area, L the length of the boundary, and the $-(+)$ refers to Dirichlet (Neumann) boundary conditions. If we take the Dirichlet boundary condition the number of eigenmodes over the concerned range is given by $N_0(11) - N_0(8) \simeq 30.0$ and for Neumann boundary condition $N_0(11) - N_0(8) \simeq 34.78$. Since under the boundary condition of the present problem both ψ and $\partial_\nu \psi$ on the boundary are nonzero, it is reasonable to find the number of resonances between those predicted in both boundary conditions. For each symmetry class we find 7 (odd-odd), 8 (odd-even), 8 (even-odd), and 10 (even-even) resonances, respectively. The smaller number of resonances for the odd-odd symmetry case and the larger

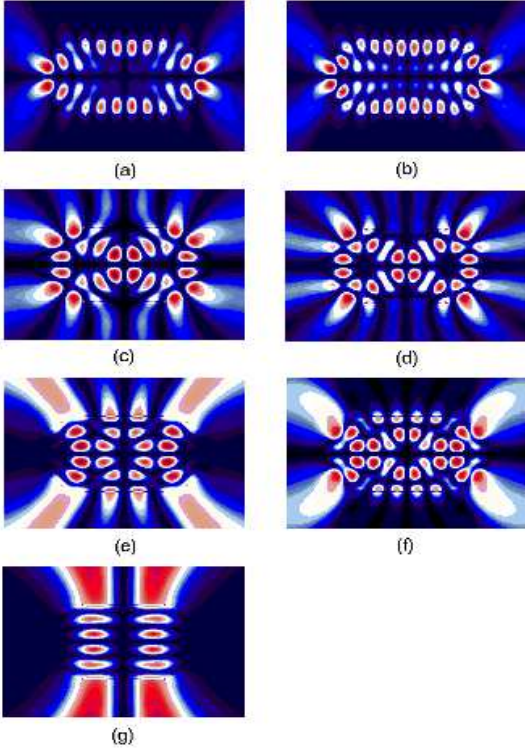


FIG. 3: (Color online) Resonances with odd-odd symmetry. (a) OO_4 , $kR = (4.67, -0.048)$ (b) OO_7 , $kR = (5.35, -0.042)$ (c) OO_2 , $kR = (4.31, -0.086)$ (d) OO_5 , $kR = (4.91, -0.076)$ (e) OO_3 , $kR = (4.49, -0.14)$ (f) OO_6 , $kR = (5.13, -0.092)$ (g) OO_1 , $kR = (4.07, -0.24)$

number for the even-even symmetry case, can be understood by Eq.(5), since the former is close to the Dirichlet boundary condition and the latter is close to the Neumann boundary condition.

The relation between Q factor and the complex wavenumber k is given by

$$Q = -\frac{\text{Re}[kR]}{2\text{Im}[kR]}. \quad (6)$$

Therefore, the smaller absolute value of imaginary part of k means the higher Q modes. Fig.2 shows all resonance positions in the concerned kR range. Black points are the resonances with odd-odd parities on x and y coordinates, respectively. This symmetry class is denoted by OO_i ($i = 1, 2, \dots$) and the index numbering starts, for convenience, from the resonance with the smallest $\text{Re}(kR)$ in the concerned range. With the same way we label other resonances, and in the figure with different color we distinguish the different symmetry classes, red, blue, and green points denote even-odd, odd-even, and even-even parities, respectively. Unlike the circular boundary in which WG modes have very small absolute value of $\text{Im}(kR)$ (e.g., $-0.0035 < \text{Im}(kR) < -0.0025$ on $\text{Re}(kR) \simeq 8$), in the stadium-shaped microcavity the high Q modes have relatively large absolute value,

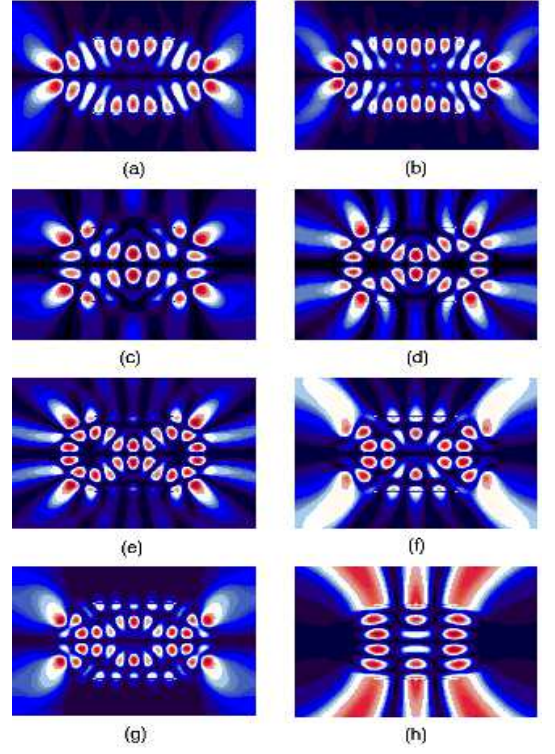


FIG. 4: (Color online) Resonances with even-odd symmetry. (a) EO_3 , $kR = (4.33, -0.053)$ (b) EO_6 , $kR = (5.01, -0.044)$ (c) EO_1 , $kR = (4.01, -0.075)$ (d) EO_4 , $kR = (4.61, -0.084)$ (e) EO_7 , $kR = (5.23, -0.073)$ (f) EO_5 , $kR = (4.80, -0.11)$ (g) EO_8 , $kR = (5.46, -0.083)$ (h) EO_2 , $kR = (4.25, -0.20)$

$|\text{Im}(kR)| \simeq 0.04$. Remember that the classical dynamics of the stadium billiard is chaotic, so it is impossible for ray to go around infinitely trapped by total internal reflection like WGM. This fact explains the absence of resonances with $|\text{Im}(kR)| < 0.03$.

It is interesting to see the relationship between patterns and $\text{Im}(kR)$ values of resonances. The resonance patterns corresponding to all resonance points in Fig.2 are drawn in Fig.3 (odd-odd parity), Fig.4 (even-odd parity), Fig.5 (odd-even parity), and Fig.6 (even-even parity). In figures color changes in order of dark blue-white-red-dark red as the intensity of electric field increases. From Figs.3-6, several resonances have similar patterns. In particular the parity on y coordinate plays more crucial role in classifying the patterns rather than the parity on x coordinate.

First let us focus on the high Q resonances for all symmetry classes. OO_4 , OO_7 (Fig.3 (a),(b)) and EO_3 , EO_6 (Fig.4 (a),(b)) are high Q modes with odd-odd and even-odd parities, respectively. It is obvious that these resonances can be classified as one class of pattern by observing the distribution of high intensity field near the boundary and same directionality of near field emission. The only difference between them is the number of intensity spots along the boundary. This fact can be il-

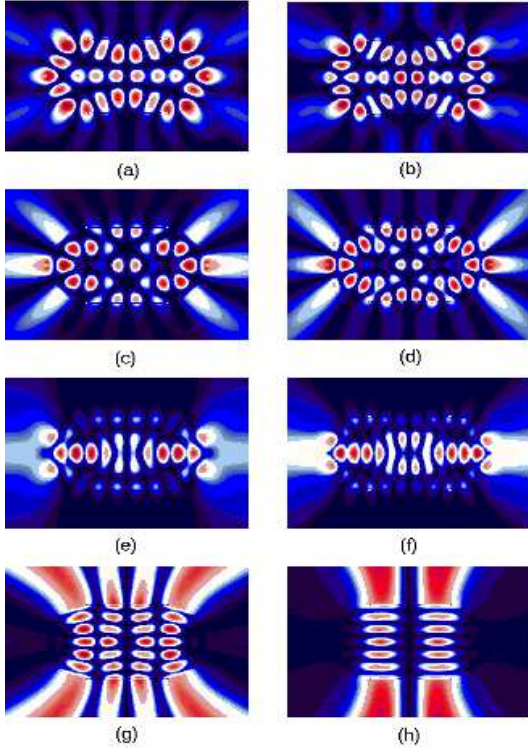


FIG. 5: (Color online) Resonances with odd-even symmetry. (a) OE_1 , $kR = (4.25, -0.040)$ (b) OE_5 , $kR = (4.89, -0.055)$ (c) OE_2 , $kR = (4.37, -0.094)$ (d) OE_6 , $kR = (5.05, -0.075)$ (e) OE_3 , $kR = (4.58, -0.10)$ (f) OE_8 , $kR = (5.32, -0.096)$ (g) OE_7 , $kR = (5.20, -0.18)$ (h) OE_4 , $kR = (4.83, -0.25)$

illustrated by almost constant difference of $\text{Re}(kR)$, i.e., $\Delta\text{Re}(kR)$ between adjacent two modes among these is about 0.34. They show very good directionality of emission. Similar discussion can be applied to the high Q modes with odd-even and even-even parities. OE_1 , OE_5 (Fig.5 (a),(b)) and EE_3 , EE_8 (Fig.6 (a),(b)) are high Q modes with odd-even and even-even parities, respectively. From the fact that the difference of $\text{Re}(kR)$ between successive modes are $\Delta\text{Re}(kR) \simeq 0.31$, we can confirm that these modes can be classified as a class. The resonance pattern of this class is somewhat different from the high Q modes of odd parity on y coordinate, high intensity spots are shown on the semicircular part of the boundary and on the central part of the cavity. We note that these patterns have high intensity on the central part. In a circular microdisk the high Q modes are WG modes which show high intensity near the boundary, indicating that the WG modes are supported by rays circulating and trapped by the total internal reflection. Although the present stadium-shaped microdisk shows chaotic ray dynamics, implying no exact WG modes trapped by total internal reflection, similar patterns are shown in the former high Q modes such as OO_4 , OO_7 , EO_3 , EO_6 . Therefore, the high intensity on the central part of the cavity in the latter high Q modes (OE_1 , OE_5 , EE_3 , EE_8) means

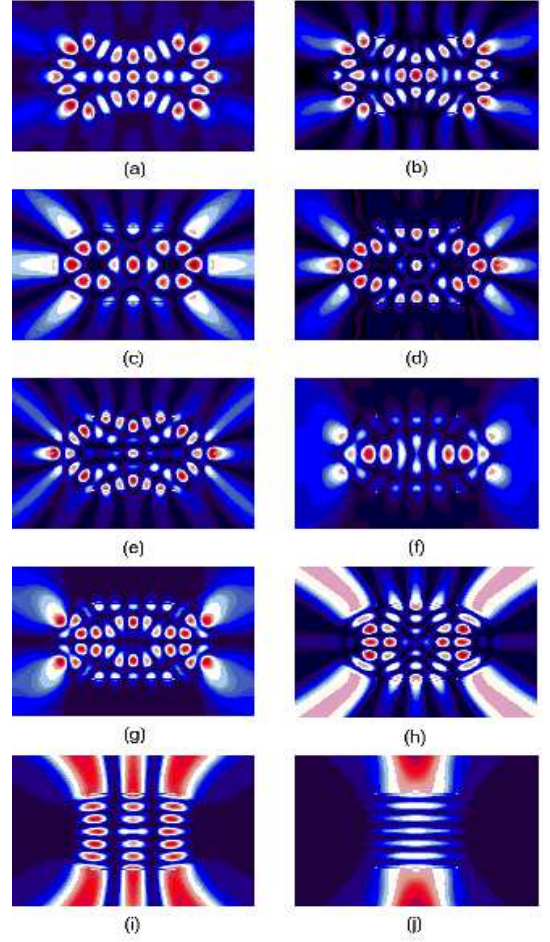


FIG. 6: (Color online) Resonances with even-even symmetry. (a) EE_3 , $kR = (4.57, -0.044)$ (b) EE_8 , $kR = (5.20, -0.065)$ (c) EE_1 , $kR = (4.04, -0.11)$ (d) EE_4 , $kR = (4.71, -0.083)$ (e) EE_9 , $kR = (5.38, -0.069)$ (f) EE_2 , $kR = (4.23, -0.10)$ (g) EE_6 , $kR = (4.95, -0.10)$ (h) EE_{10} , $kR = (5.47, -0.13)$ (i) EE_7 , $kR = (4.98, -0.22)$ (j) EE_5 , $kR = (4.74, -0.27)$

that rays supporting those modes are different from those for the WG type resonances, and they would pass the central part of the cavity. The ray dynamical consideration for the high Q modes would be presented in Sec.VI.

Next we consider other pattern classes of resonances in the same $\text{Re}(kR)$ range. EO_1 , OO_2 , EO_4 , OO_5 , and EO_7 form a class of pattern which has attached two circle structure inside the boundary and $\Delta\text{Re}(kR) \simeq 0.3$. EE_1 , OE_2 , EE_4 , OE_6 , and EE_9 show similar two circle structure with one line of spots near the straight segments of the boundary, giving $\Delta\text{Re}(kR) \simeq 0.33$. EE_2 , OE_3 , EE_6 , and OE_8 have a simple line structure, the high intensity spots are concentrated on the x -axis, giving $\Delta\text{Re}(kR) \simeq 0.36$. OO_3 , EO_5 , OO_6 , and EO_8 show low intensity on the center of the stadium, giving $\Delta\text{Re}(kR) \simeq 0.32$. The very high loss (large $|\text{Im}(kR)|$) resonances are OO_1 , EO_2 , EE_5 , OE_4 , EE_7 and OE_7 which are basically bouncing ball type resonances.

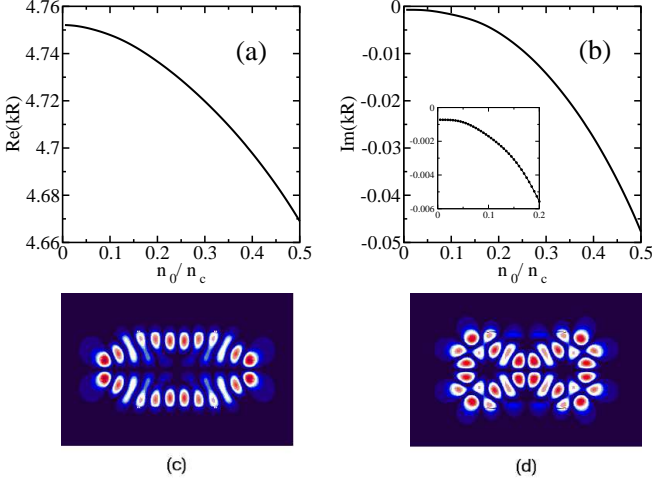


FIG. 7: (Color online) Variation of resonance with n_c . (a) Variation of $\text{Re}(kR)$ of the resonance mode OO_4 . (b) Variation of $\text{Im}(kR)$ of the resonance mode OO_4 . The inset show the convergence of $\text{Im}(kR)$ to a nonzero value clearly when $N = 50$. (c) The limiting resonance of the mode OO_4 (at $n_0/n_c = 0.01$). (d) The limiting resonance of the mode OO_5 (at $n_0/n_c = 0.01$).

From the patterns we can find general rules about the relationship between intensity distribution of patterns and $|\text{Im}(kR)|$ values. As discussed before, the high Q modes (low value of $|\text{Im}(kR)|$) show localized patterns near the boundary or the center of the stadium-shaped microdisk cavity. As $|\text{Im}(kR)|$ value increases, the high intensity spots move toward inside the cavity and emission from cavity becomes clear, reflecting higher energy loss. The modes with highest energy loss, corresponding to the large $|\text{Im}(kR)|$ values, are the bouncing ball type patterns.

In usual experimental situations, it is hard to directly observe either the resonance pattern inside microcavity or the near field distribution. Therefore the far field distribution of resonance would be a convenient physical quantity with which one can distinguish different resonance modes in experiments. Similar to the previous pattern classification, the far field distributions of the resonances are also, although less obvious, classified, and they are roughly expected from the extension of the corresponding near field distributions. For example, the high Q modes in the odd-odd and even-odd symmetry classes (Fig.3 (a),(b) and Fig.4. (a),(b)) show good directional emission at about 40° from the x -axis in the far field distribution, while the high Q modes in the odd-even and even-even symmetry classes (Fig.5 (a),(b) and Fig.6 (a),(b)) have oscillatory far field distributions implying several emitting beams over rather wide angle range.

IV. PATTERN CHANGE WITH REFRACTIVE INDEX

In this section we study the pattern change of resonances with varying refractive index n_c . Sometimes it seems to be accepted as a general concept that the high refractive index limit ($n_c \rightarrow \infty$) in microcavity would be equivalent to the infinite wall case (usual billiard systems). This might be based on the following reasoning. Since in higher n_c case the critical angle for total internal reflection is very small, and approaches to zero in the limit, rays are confined in the cavity by the total internal reflections. This situation is very similar to the infinite wall case. One would, therefore, expect that patterns of eigenfunctions of the infinite wall case would represent the limiting ($n_c \rightarrow \infty$) patterns of resonances.

Here we examine this expectation by observing changes of the complex wavenumber k and resonance pattern with increasing the refractive index n_c inside the cavity and by comparing the limit values with the eigenvalues of the infinite wall case. In order to keep the number of intensity spots in resonance patterns, we scale the size of the microcavity so that $n_c R$ remains constant. In Fig.7 is shown the evolution of resonance position kR of the resonance mode OO_4 . The $\text{Re}(kR)$ converges to about 4.752 and the $\text{Im}(kR)$ seems to approach zero as n_c increases. In fact, it is very difficult to say definitely if the $\text{Im}(kR)$ become zero at the limit or not, due to the numerical error in BEM. The inset in Fig.7 (b) shows the saturation behavior to a nonzero value of $\text{Im}(kR)$ when $N = 50$, but if we increase the number of elements, the saturation value gets closer to the real axis with a convergence slower than logarithmic one. We also calculate eigenvalues of the stadium billiard in the concerned range which are $kR = 4.23, 4.44, 4.81, 4.86, 5.12, 5.46$. We note that any of them does not coincide with the limiting value 4.752, which mean that, although the imaginary part of the wavenumber kR gets closer to real axis, the resonance never approaches an eigenmode of the infinite wall case. This result can be understood in terms of the evanescent effect, i.e., tunneling effect, in the dielectric microcavity system. In the infinite wall case, the evanescent effect is not allowed by the Dirichlet boundary condition, and no amplitude outside the boundary. Although the classical dynamics is similar, the evanescent effect can appear in the microcavity case, because rays can exist outside as well as inside the cavity. The same argument is available for the WGM in which the small emission from the cavity is the result of the evanescent effect. From this reasoning we guess that there would be very small nonzero limiting value of $\text{Im}(kR)$ due to the evanescent effect.

The resonance pattern with $n_0/n_c = 0.01$, n_0 is the refractive index outside the cavity ($n_0 = 1$ in our case), is shown in Fig.7 (c). The pattern inside the cavity has no crucial difference from the $n_c = 2$ case when compared to Fig.1 (a), and the emission pattern outside the cavity is drastically reduced, reflecting the strong ray confinement. This behavior is also true for other resonances,

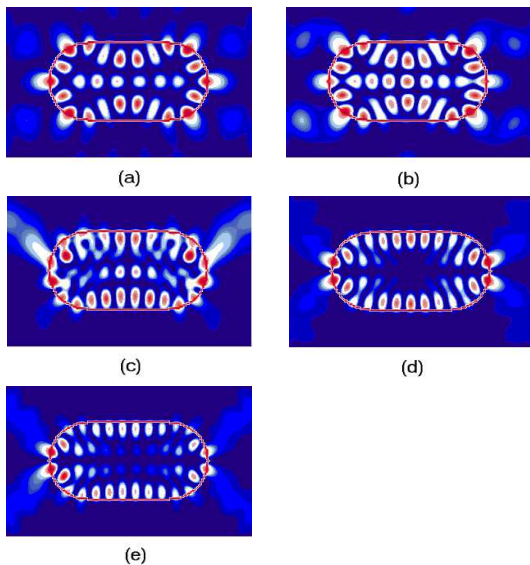


FIG. 8: (Color online) Stationary lasing modes with low pumping rates in the nonlinear dynamical model. The center positions of the gain profile are on $\text{Re}(kR) = 4.3$ (a), $\text{Re}(kR) = 4.7$ (b), $\text{Re}(kR) = 4.9$ (c), $\text{Re}(kR) = 5.1$ (d), and $kR = 5.3$ (e). The corresponding resonances are the high Q modes, (a) OE_1 , (b) EE_3 , (c) $OO_4 + OE_5$, (d) EO_6 , and (e) OO_7 .

and the limiting pattern of OO_5 is also shown in Fig.7 (d).

V. DYNAMICAL MODELING OF MICRODISK LASER

Conceptually, a dynamical description of the microdisk laser is the same as that of any other type of laser: it should include equations for material polarization and inversion of the active medium and equations for electromagnetic field. Of these equations, only the field equations require a special treatment in the case of the microdisk laser. The main difficulty is that an analytical description of resonant mode functions, their frequencies and linewidths is generally impossible. Even if all these data are known from independent calculations, for example, obtained by using BEM as in previous chapters, it is not obvious which of these modes should be included into the model to incorporate the main features of the microdisk laser dynamics. One can, of course, include into the model all the resonances whose frequencies fall into the positive gain range of the active medium. However, such an approach can encounter numerical problems, especially for sufficiently large cavities and wide spectral contour gain.

An alternative approach to the problem was proposed by Harayama et al.[14]. They developed a model for the microdisk laser and called it "Schrodinger- Bloch model". In their derivation of the Schrodinger-Bloch model equations the authors made an approximation, replacing the

space-dependent refractive index in some expression by a constant value. Using this model Harayama et al. have found that lasing patterns obtained are in a very good agreement with the BEM results. However, the authors did not discuss the question, why the effect of the refractive index replacement, made to derive the Schrodinger-Bloch model equations, is as minor.

Our results presented in Sec.IV, allow us to clarify this question. Actually, the replacement mentioned above is equivalent, in a sense, to the refractive index change described in Sec.IV. Fig.7 shows clearly that the pattern and the wavelength location of the resonance do not change significantly with refractive index. However, the situation is quite different for the width of the resonance, i.e. for the mode damping : it is highly sensitive to refractive index variations. This behavior is quite similar to that of conventional Fabry Perot resonator[18], for which mode frequencies are determined by its length and mode damping - by the reflectivity of mirrors. So, we believe that the accuracy of the threshold characteristics obtained using the Schrodinger-Bloch model are not of high accuracy. However, we believe that the relative positions of resonances shown in Fig.2 do not change.

Keeping this discussion in mind, we use the Schrodinger-Bloch model to simulate the stadium-shaped microdisk laser in the oscillating regime. The material parameters used correspond to semiconductor active medium. The polarization relaxation time $T_2 = 50fs$ is typical for charge carrier concentration $n \simeq 10^{18}cm^{-3}$. For the wavelength near $\lambda = 0.86\mu m$ and $\text{Re}(kR) = 4.3$ we get the FWHM of the optical transition $\Delta\text{Re}(kR) = 0.08$. The transition dipole matrix element $p = 15D = 1.5 \times 10^{-17}CGS$ corresponds to semiconductor quantum well structures. A typical value for the excited state relaxation time for semiconductors is $T_1 = 10^{-19}sec$, but we used in simulations ten or more times lower values. We can get various stationary lasing modes whose basic patterns can be found in the resonance patterns presented in Fig.3-6. The stationary lasing modes with low pumping rates are shown in Fig.8. When the gain profile is centered on $\text{Re}(kR) = 4.3$, the resonance mode OE_1 is excited as the lasing mode. As shown in Fig.2, it is consistent with the fact that the highest Q mode near $\text{Re}(kR) = 4.3$ is the mode OE_1 . The same argument is valid for other cases, i.e., when the position of the gain profile are $\text{Re}(kR) = 4.7, 5.1$, and 5.3 , the stationary lasing modes are the high Q resonance modes, EE_3 , EO_6 , and OO_7 , respectively. The asymmetric lasing mode shown in Fig.8 (c) can arise from the multimode lasing with different symmetry classes, i.e., the resonance modes OO_4 and OE_5 . The direction of asymmetric emission oscillates, upwards and downwards alternately. We can expect if the pumping rate increase, this multimodes operation becomes single mode operation resulted from the locking process[15].

From the above calculation for the active microcavity, we can see that the interaction between field and active medium does not give any substantial pattern change

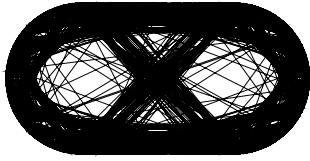


FIG. 9: The 50 trajectories with long path length, $l_{es} > 40$, when $R = 1$, before escaping.

from the resonance patterns of the passive microcavity. This result means that the analysis of the resonance patterns of the passive microcavity shown in Sec.III would play an essential role in understanding the lasing modes from the active microcavity.

VI. CLASSICAL CONSIDERATION BASED ON RAY DYNAMICS

It is well known that the stadium system is classically chaotic, so there is no special structure in the portrait of the Poincaré surface of section, showing just chaotic sea over the whole phase space. However, in the dielectric cavity case rays can escape the cavity. The path length before the escape should depend on the initial point in the phase space, and we can obtain some structure related to the path length in the phase space.

From the fact that the WGM of very high Q factor in the circular disk are supported by the rays surviving infinitely through the total internal reflection, we can expect that the high Q modes would be supported by the rays with long path length before the escaping by refraction. We select 50 initial points from which the generated ray trajectories have long path length, $l_{es} > 40$, when $R = 1$, before escaping. The trajectories starting from the 50 initial points are shown in Fig.9. We can see that the trajectories with long path length pass near the boundary and the center of the stadium which coincide with the high intensity regions in the high Q resonances. Similarly, the low Q resonance modes of bouncing ball type are supported by the rays with short path length before escaping.

More generally, we can consider some distributions

over the phase space to characterize the ray dynamical behavior in microcavities, e.g., the path length distribution $D(s, p)$ and the survival probability distribution $\tilde{P}(s, p, t)$. The path length distribution $D(s, p)$ can be given by the characteristic length of the trajectory starting from an initial point (s, p) . Therefore, if the initial point is on a periodic orbit (s_p, p_p) and the absolute values of associated p values are greater than the critical value p_c of the total internal reflection, the value of $D(s_p, p_p)$ becomes infinity. Since the trajectories starting from the initial points near the stable manifold around the periodic orbit would have long characteristic lengths, the structure of $D(s_p, p_p)$ would follow the structure of the stable manifold. On the other hand, when we consider an ensemble of uniform initial points over the whole phase space, we can trace the flow of the points in the phase space and after long time due to energy escape by emission the points with lower weight are redistributed, and as a result a steady probability distribution can be achieved. This steady probability distribution can be approximated by the normalized survival probability distribution $\tilde{P}(s, p, t)$ at a long time[13]. This distribution would be closely related to the high Q resonance patterns and have the structure of unstable manifolds.

VII. SUMMARY

Using the BEM, we obtained all resonances in the range of $4 < \text{Re}(kR) < 5.5$ for the stadium-shaped microdisk, and investigated the patterns of high Q resonances for four different symmetry classes. The high Q resonances show high intensity distribution near the boundary and central part of the cavity, which is consistent with the classical ray consideration. The relationship between Q value and resonance pattern was discussed, and the resonances could be classified by the difference of the patterns even though the classical dynamics is chaotic. We also confirmed that the stationary lasing modes with low pumping rate in the nonlinear dynamical model are the high Q modes. From this resonance pattern analysis, we can expect which type of pattern can be excited as a stationary lasing mode.

VIII. ACKNOWLEDGEMENTS

This work is supported by Creative Research Initiatives of the Korean Ministry of Science and Technology.

-
- [1] *Optical Processes in Microcavities*, edited by R. K. Chang and A. J. Campillo (World Scientific, Singapore, 1996).
 - [2] S. L. McCall, A. F. J. Levi, R. E. Slusher, S. J. Pearton, and R. A. Logan, Appl. Phys. Lett., **60**, 289 (1992).

- [3] R. E. Slusher, A. F. J. Levi, U. Mohideen, S. L. McCall, S. J. Pearton, and R. A. Logan, Appl. Phys. Lett., **63**, 1310 (1993).
- [4] L. Collot, V. Lefevreseguin, M. Brune, J. M. Raimond,

- and S. Haroche, Europhys. Lett., **23**, 327 (1993).
- [5] T. Harayama, P. Davis, and K. S. Ikeda, Phys. Rev. Lett. **82**, 3803 (1999)
 - [6] J. U. Nöckel and A. D. Stone, Nature **385**, 45 (1997).
 - [7] H. G. L. Schwefel, N. B. Rex, H. E. Tureci, R. K. Chang, and A. D. Stone, arXiv:physics/0308001 (2003).
 - [8] S. Chang, J. U. Nöckel, R. K. Chang, and A. D. Stone, J. Opt. Soc. Am.B **17**, 1828 (2000).
 - [9] S.-B. Lee, J.-H. Lee, J.-S. Chang, H.-J. Moon, S. W. Kim, and K. An, Phys. Rev. Lett. **88**, 033903 (2002).
 - [10] C. Gmachl, E. E. Narimanov, F. Capasso, J. N. Bal-largeon, and A. Y. Cho, Opt. Lett. **27**, 824 (2002).
 - [11] N. B. Rex, H. E. Tureci, H. G. L. Schwefel, R. K. Chang, and A. D. Stone, Phys. Rev. Lett. **88**, 094102 (2002).
 - [12] T. Harayama, T. Fukushima, P. Davis, P. O. Vaccaro, T. Miyasaka, T. Nishimura, and T. Aida, Phys. Rev. E **67**, 015207(R) (2003).
 - [13] S.-Y. Lee, S. Rim, J.-W. Ryu, T.-Y. Kwon, M. Choi, and C.-M. Kim, arXiv:nlin.CD/0403025 (2004).
 - [14] T. Harayama, P. Davis, and K. S. Ikeda, Phys. Rev. Lett. **90**, 063901 (2003).
 - [15] T. Harayama, T. Fukushima, S. Sunada, and K. S. Ikeda, Phys. Rev. Lett. **91**, 073903 (2003).
 - [16] J. Wiersig, J. Opt. A: Pure Appl. Opt. **5**, 53 (2003).
 - [17] H. P. Baltes and E. R. Hilf, *Spectra of Finite Systems*, (B. I. Wissenschaftsverlag, Mannheim, 1976).
 - [18] N. Hodgson, H. Weber. *Optical Resonators: fundamentals, advanced concepts, and applications*. (Springer-Verlag London, 1997).